EUROPEAN FUSION DEVELOPMENT AGREEMENT

EFDA–JET–PR(03)03

J. Paméla, Emilia R. Solano and JET EFDA Contributors

Overview of JET Results

Overview of JET Results

J. Paméla[1], E.R. Solano[1] and JET EFDA Contributors*

[1]EFDA Close Support Unit, Culham Science Centre, Abingdon, Oxon, OX14 3EA, UK
** See Annex 1 of J. Paméla et al, 'Overview of JET Results'*

Preprint of Paper to be submitted for publication in
Nuclear Fusion

ABSTRACT.

Scientific and technical activities on JET focus on the issues likely to affect the ITER design and operation. Understanding of the ITER reference mode of operation, the ELMy H-mode, has progressed significantly. The extrapolation of ELM size to ITER has been re-evaluated. Neoclassical Tearing Modes have been shown to be meta-stable in JET, their beta limits can be raised by destabilisation (modification) of sawtooth by ICRH. Alpha simulation experiments with ICRH accelerated injected ^{4}He beam ions provide a new tool for fast particle and MHD studies, with up to 80–90% of plasma heating by fast ^{4}He ions. With or without impurity seeding, quasi-steady state high confinement ($H_{98} = 1$), high density ($n_e/n_{GR} = 0.9$–1) and high β ($\beta_N = 2$) ELMy H-mode has been achieved by operating near the ITER triangularity ($\delta \sim 0.40$–0.5) and safety factor ($q_{95} \sim 3$), at $Z_{eff} \sim 1.5$–2. In Advanced Tokamak scenarios, internal transport barriers (ITBs) are now characterised in real time with a new criterion, ρ^*_T. Tailoring of the current profile with LHCD provides reliable access to a variety of q profiles, lowering access power for barrier formation. Rational q surfaces appear to be associated with ITB formation. Alfvén cascades observed in Reversed Shear plasmas, providing identification of q profile evolution. Plasmas with 'current holes' were observed and modelled. Transient high confinement Advanced Tokamak regimes with $H_{89} = 3.3$, $\beta_N = 2.4$ and ITER relevant $q < 5$ were achieved with reversed magnetic shear. Quasi-stationary internal transport barriers are developed with full non-inductive current drive, including ~50% bootstrap current. Record duration of ITBs was achieved, up to 11 s, approaching the resistive time. For the first time, pressure and current profiles of Advanced Tokamak regimes are controlled by a real time feedback system, in separate experiments. Erosion and co-deposition studies with the quartz-micro-balance show reduced co-deposition. Measured divertor thermal loads during disruptions in JET could modify ITER assumptions.

1. INTRODUCTION

With its divertor configuration, plasma size, heating, current drive and diagnostic systems, Tritium, Beryllium and remote handling capabilities, the JET device can access a wide range of operating regimes in experimental conditions closest to those of a burning plasma experiment. Prior to and during the design phase of ITER, JET produced major contributions to the ITER Physics Basis [1] used to extrapolate plasma performance to ITER. In the last two years, the JET research programme has focused on issues critical to finalise the details of the ITER design and prepare its operation.

The shaping capability of JET has been extended toward plasma shaping very close to that of ITER, in particular with high triangularity, $\delta \sim 0.5$, achieved at up to 2.5 MA. Relevant higher current experiments require higher power, expected to be available in future experimental campaigns. The shaping capability has been further extended by the removal of dome and septum from the MarkII-GB divertor. Operating at or near the foreseen ITER plasma shape has proven essential, due to the strong effect of parameters like triangularity on Edge Localised Modes (ELMs), ELMy H-mode performance at high density and advanced modes. ITER operational scenarios can be optimised

in a highly relevant and consistent range of parameters simultaneously achieved (δ, κ, q_{95}, as well as ρ^*, ν^* etc.).

In addition, diagnostic and analysis capabilities have been improved. New or upgraded diagnostics commissioned in the last 2 years include correlation reflectometry, Electron Cyclotron Emission (ECE) profile system, Quartz Micro-Balance (QMB), improved Motional Stark Effect (MSE), shape controller upgrade, halo current diagnostics and pellet spectrometers. The real time control system has been developed, and proved to be successful in demonstrating the capability to control pressure or current profiles of plasmas with Internal Transport Barriers.

This overview paper presents only a selection of recent JET results, first concentrating on advances in the two main operating regimes foreseen on ITER, the ELMy H-mode and Advanced Tokamak scenarios, and then describing new results in various operating regimes. More details, as well as other results, can be found in accompanying papers in this issue [2, 3, 4, 5, 6, 7, 8, 9, 10, 11, 12, 13, 14, 15, 16, 17, 18, 19].

2. ELMY H-MODE

One of the key scientific programmes conducted on JET is dedicated to further consolidating the ITER reference scenario, the ELMy H-mode [20,21]. ELM studies are presented in Section 2.1, followed in Section 2.2 by key MHD and fast particle issues, such as NTMs and α-simulation investigated in ELMy H-modes. Section 2.3 summarises performance achievements: high confinement at high density and high β.

2.1. EDGE LOCALISED MODES (ELMS)

Dedicated studies have investigated ELM size scaling [2], power loads at the divertor target [3], techniques for ELM amelioration and mitigation [4], MHD stability and characteristics of ELMs in Advanced Tokamak scenarios [7]. The new expectations for Type I ELMs in ELMy H-mode in ITER now span the tolerable range.

2.1.1. Scaling of ELMs with pedestal characteristics, ITER predictions

Characterisation of the pedestal region in JET ELMy H-mode with Type I ELMs shows that typically the plasma pressure collapses in about the outer 15–20% of the outer plasma minor radius in a ~ 200 μs time-scale. Increasing the $n_{e,\,ped}$ decreases the relative drop in $T_{e,\,ped}$ (conductive ELM loss) but not in $n_{e,\,ped}$ (convective ELM losses). For some configurations Type I ELMs are identified, in which the ELM energy losses are purely convective [22].

New results at high δ in JET experiments have shown a break of the relation between Type I ELM frequency and size with increasing pedestal density, as illustrated in Figure 1. At high $n_{e,\,ped}$ a decrease of f_{ELM} is observed together with a slight decrease of ΔW_{ELM}. This anomalous behaviour of the Type I ELM frequency is associated with an enhanced level of fluctuations in-between Type I ELMs with similar characteristics to those seen in Type II ELMs [23]. The anomalous ELM

behaviour has been instrumental in demonstrating that the ELM energy loss is determined by the values of the pedestal plasma parameters while the ELM frequency is a consequence of the in-between ELM transport. An empirical correlation was found between the normalised Type I ELM energy loss (to the pedestal energy), $\Delta W_{ped}/W_{ped,}$ and the pedestal plasma collisionality, for a large range of plasma conditions, as shown in Figure 2. Alternatively, the $\Delta W_{ped}/W_{ped}$ data is also well ordered by the ion transit time along the connection length, $\tau_{||ion}$, calculated with ion pedestal values. This could be related to the impedance for heat flux through the divertor target sheath during the ELM, and the connection of the pedestal plasma with the divertor target along 'broken' field lines [24].

Estimates of expected divertor lifetime in ITER have been reviewed and modified [3, 25], as data from JET, other devices and material tests provided a more refined basis for modelling of acceptable ELM power load on target components. The vertical arrows on Figure 2 mark the present estimates of the acceptable ELM energy in ITER, assuming either 60% or 100% of plasma energy loss arrives at the target (50–80% observed at JET). The upper and lower values in each range originate from differences in the assumptions of ELM power deposition and ITER divertor target options [25].

2.1.2. Impurity seeding for ELM mitigation

ELM mitigation by impurity seeding has been demonstrated in JET [4, 9]. With Ar, in Type I ELMy H-modes, the increase in edge radiated power leads to a reduced target peak heat load, measured by IR thermography of the divertor target plates. Ar seeding leads to a decrease of the ELM frequency and a reduction in $\Delta W_{ELM}/W_{ped}$, correlated with a change of the pedestal parameters, as can be seen in the Ar seeded data presented in Figure 2.

2.1.3. MHD stability of the H-mode edge pedestal

The stability of H-mode edge pedestals has been analysed considering medium to large n kink/ballooning modes [23, 26] and including stabilising diamagnetic effects [27]. In the second stable regime for infinite n ballooning modes, the medium-n ballooning modes set the actual limit on the pressure gradient: higher than 1st stability, but not second stable. Integrated transport/MHD modelling is being used to study the effect of edge density on plasma collisionality and therefore on bootstrap current and stability. The JETTO predictive transport code has been connected with the MISHKA and IDBALL MHD codes, so ELM models can be explored [5]. Study of ELM precursors and post-cursors and inter-ELM activity is on-going [6, 28]

2.1.4. ELMs in AT scenarios

Controlling ELMs is important in Advanced Tokamak (AT) scenarios, as large Type I ELMs can destroy the ITB [29]. In typical AT discharges in JET, Type-III ELMs can be maintained at heating powers exceeding the threshold for the Type-III to Type-I ELM transition in H-mode by a factor of

2 [30]. This observation lead to a study of the effect of current ramps in high (ITER-relevant) triangularity discharges, showing that the edge stability is modified and type I ELMs can be suppressed in AT scenarios [7].

2.2. CORE MHD ISSUES IN ELMY H-MODE

In ELMy H-mode discharges, core MHD, which can depend on kinetic effects, can have an impact on confinement.

2.2.1. Sawteeth and NTMs

In JET, it has long been known that MHD activity triggered by large sawteeth can reduce confinement. Notably, during the JET DT campaign, sawtooth control raised fusion power by 30% from a saturated value of 10 MW. This was obtained by delaying the sawtooth crash (fine-tuning the gas puff rate), and therefore avoiding confinement degradation. Recent modelling shows that fast particle stabilisation lead to larger sawteeth, triggering NTMs and reducing confinement in these fusion-relevant plasmas [31]. This lends credibility to α-simulation, discussed later in this section, where equivalent evolution is observed.

Concern about the effect of NTMs on confinement in ITER prompted a series of studies in JET on NTM stability, in ELMy H-mode plasmas [8, 32]. It is found that the onset β-limits for NTMs depend very much on the seeding process. Most commonly the NTM seed perturbation is a sawtooth, suggesting the opportunity for NTM control via control of the sawtooth seed. Detailed scans have shown that heating and current drive from 2^{nd} harmonic Ion Cyclotron Radio Frequency (ICRF), when located near the sawtooth inversion radius, causes small frequent sawteeth. In a seminal experiment this sawtooth control has been exploited to raise the 3/2 NTM onset β-limit in JET discharges up to $\beta_N = 3.6$ [33]. Conversely it is found that long period sawteeth are found to result in a low onset β_N for the 3/2 NTM, as shown in Figure 3 (partly derived from [34]). By generating long period sawteeth, generally by ICRH fast particle stabilisation, NTMs can be accessed at high toroidal field in JET; allowing the properties of NTMs to be studied at ρ^* values to within a factor of ~1.5 of the ITER Q = 10 value (albeit at lower β_N values where the confinement degradation effects of the NTMs are modest). Direct power-law type extrapolations for the onset β_N are of dubious value, given the nonlinearities introduced by the seeding process. However studies of the marginal-β (below which the NTMs are unconditionally stable), as opposed to the onset β_N, are not complicated by the effects of the seeding process. Such studies reveal that typical H-mode conditions in JET are metastable to 3/2 NTMs (which is why long period sawteeth can generate NTMs at low β_N), and initial scalings further indicate that the same will be true in ITER [35], where NTMs may then be generated by long period sawteeth occurring due to α-particle stabilisation effects. Overall these results indicate the importance of developing NTM control strategies for ITER, and of further studying the physics of the seeding process to predict onset-β_N limits for ITER; JET is well placed to make such studies in ITER relevant regimes with access to low ρ^* and large sawteeth.

2.2.2. α-simulation

On-axis ion cyclotron resonance heating (ICRH) of neutral beam injected ^{4}He ions (3rd harmonic) produced a high-energy population of ^{4}He ions which simulate 3.5 MeV fusion-born alpha particles [36]. Strongest tails were created with highest energy ^{4}He seed beams, as expected. In these stationary plasmas, fast ^{4}He provided up to 80–90% of plasma heating. The successful acceleration of ^{4}He beam ions to the MeV energy range was confirmed by measurements of γ-ray emission (see Section 4.1.1) [37] and excitation of Alfvén eigenmodes [10, 38], and was consistent with the observed heating of the background electrons and sawtooth stabilisation. This experiment provided yet another example of the interconnection between various physical mechanisms: fast particles stabilise sawteeth, which acquire large amplitude, trigger NTMs, and confinement is degraded [see 8]. The scheme can now be used in forthcoming JET campaigns with ^{4}He plasmas for dedicated alpha-particle studies.

2.3. INTEGRATED ELMY H-MODE SCENARIOS

High performance ELMy H-mode integrated scenarios have been achieved with various methods [9, 20], as displayed in Table I and described in Sections 2.3.1–2.3.4. At reduced performance, a simulation of fusion burn dynamics was undertaken, described in Section 2.3.5.

2.3.1. High confinement at high density, achieved with high triangularity, high power

Experiments studying the beneficial effect of high triangularity [23] and high heating power [39] on confinement have confirmed and extended earlier results, demonstrating high H factor at high density, as shown in Table I. These discharges have single lower null, with ion grad B drift towards the X-point, standard q profile, NBI heating and gas fuelling. The separatrix geometry was similar to that envisaged for the standard Q = 10 operation in ITER, with average triangularity $\delta \sim 0.45$–0.5 and elongation $\kappa \sim 1.75$. Figure 4 illustrates the beneficial effect of high triangularity on confinement at high density, up to the Greenwald density (n_{GR}).

Table I: Performance achievements in ELMy H-mode in JET

	High δ, high power #53299 (Type I-II)	*High δ, Ar seeding #53550, Type I*	*ITER*
$H_{98(y,\,2)}$	0.91	0.96	1.0
$\beta_{N,\,th}$	2.0	2.0	1.81
f_{GWD}	1.1	1.0	0.85
Z_{eff}	1.5	2.2	1.7
P_{rad}/P_{tot}	0.4	0.7	0.58
κ, δ	1.74, 0.48	1.7, 0.4	1.84, 0.5
q_{95}	3.2	3.1	3.0
τ_{pulse}/τ_E *	15	10	110

* Limited by technical constraints only.

In those high δ, high density plasmas, a decrease of the Type I ELM frequency with density is observed, associated with high pedestal density: $n_{ped.} \geq 70\% n_{GR}$. The reduction of f_{ELM} is associated with high frequency fluctuations in the D_α emission (and enhanced D_α baseline level) in the inter-ELM period, accompanied by the appearance of a characteristic broadband MHD turbulence and by an increase of the density fluctuations in the pedestal region. This inter-ELM activity is also associated with high pedestal pressure and increased plasma power losses (see Section 2.1.1). The comparison with results from AUG [40] suggests that those high frequency D_α oscillations could be identified as Type II ELMs. Plasmas where Type I and Type II ELMs coexist are also observed in both AUG and JT-60U [41], when the critical parameters for the complete suppression of Type I ELMs are approached.

2.3.2. Impurity seeding

Stationary high performance phases (up to 12 τ_E) have been obtained with impurity seeding, simultaneously satisfying or exceeding the ITER Q =10 ELMy H-Mode requirements for $H_{989(y, 2)}$, f_{GWD} and β_N [9], as shown in Table I. In low δ plasmas, with the X-point on the septum, there is a pronounced peaking of the electron density profile. In high δ plasmas, the formation of a radiating belt inside the separatrix has been clearly established with high radiative power fractions up to 70%. Central impurity accumulation was avoided by application of ICRF heating, maintaining the safety factor on axis below 1, so sawteeth expelled impurities [42].

2.3.3. High confinement at high density, obtained by pellet injection

An optimized pellet sequence has been developed, consisting of a first phase where the density is increased (while allowing a small confinement loss) followed by a second phase minimizing the particle flux in order to maintain the density and to recover confinement. In this way, simultaneously $H_{98(y, 2)} \sim 0.8$ with $\beta_N > 1.8$ and $f_{GWD} \sim 1$ have been reached, albeit not yet under stationary conditions. The plasma density profile shows a large peaking with $n/n_{ped} = 2$ and a decrease of Z_{eff} to about 1.7 is obtained at the highest densities reached [43].

2.3.4. Density peaking

Long time-scale density peaking has been observed in JET plasmas leading to densities exceeding the Greenwald value [44]. These neutral beam heated discharges are characterised by type-I ELMs and good energy confinement. The central density is limited by NTMs or by termination of the H-mode, preceded by loss of sawteeth. When these limiting factors are avoided (i. e. at intermediate power level and with optimisation of gas puffing) quasi-stationary high density plasmas with peaked density profiles are obtained. Whether the peaking is associated with an anomalous pinch is an issue still being investigated.

Analysis shows that this density peaking is consistent with the Ware pinch if the ratio of particle and heat diffusivity is $D/\chi_{eff} \sim 0.25$. Assuming a strong anomalous pinch, of order $V = 10 \times V_{Ware}$,

would result in a particle diffusion coefficient of order $D/\chi_{eff} \sim 1$. The modelling of a large number of density profiles in H-mode did not allow discrimination between these two hypothesis. On the other hand an anomalous particle pinch must be invoked to explain the evolution of the density profile in L-mode, in particular with pellet injection [45]. In H-mode, simulations of ITG/TEM turbulence exhibit a clear anomalous pinch. Results in L and H modes may be reconciled by noting that a core H-mode plasma is less turbulent than in L-mode. The actual pinch velocity is the sum of neoclassical and turbulent contributions, whereas the diffusion coefficient is essentially the turbulent one. The Ware pinch is therefore dominant in quiescent plasmas. This hypothesis is currently under investigation at JET.

2.3.5. Scaling laws

The influence of peaking, triangularity and proximity to the Greenwald limit on energy confinement scaling has been investigated and has a minor effect on confinement predictions for ITER (<10% in τ_E) [46]. A set of experiments in He [47] (with purity $C_{He}/C_D = 85\%$) added to our knowledge of the scaling of confinement with Z: $\tau_E \propto Z^{-0.59}$. The L-H threshold power in He plasmas shows the same B_t and n_e dependence as in D plasmas, but is 50% higher in absolute value.

A two term scaling law has been developed in the frame of the ITPA H-mode Database Working Group [46]. The best fit for an ELMy-H mode is compatible with an L-mode core and a pedestal confinement that depends sensitively on β. This finding is not compatible with strongly stiff profiles since in this case the central temperature is proportional to the pedestal height. The question of stiffness has been investigated on both experimental [11, 17] and theoretical sides. ICRH modulation experiments with mode conversion in L mode show the existence of a threshold for electrons [12]. For ions evidence has been obtained from steady-state profiles in H mode [48]. In general a transport model based on a critical gradient gives a satisfactory prediction of confinement, but with a moderate stiffness factor. In such case, the global confinement time obtained with the values of instability threshold and medium stiffness factor found in JET is compatible with the ITPA two term scaling law.

2.3.6. Burn control simulation

ICRH, via fast ions, mainly heats the electrons and is centrally deposited. These are characteristics of plasma self-heating from alpha particles. An experiment was devised in which a component, $P_{a,\,sim}$, of the ICRH heating was made proportional to a scaled fusion reaction rate (proportional to n^2). A separate component of either ICRH or NBI was used in the role of auxiliary power, P_{aux}. The discharge trajectories were programmed to simulate a reactor situation approaching ignition: magnetic field, power level and density were all chosen to lead to an L-H transition towards the end of the P_{aux} ramp, when the sum $P_{aux} + P_{\alpha,\,sim}$ reaches the L-to-H transition power threshold. The real time control system acted on the P_{aux} heating component to control the burn, precluding a 'thermal runaway', as shown in Figure 5. More details on these experiments are presented in [11, 49, 50].

2.4. FUTURE PLANS, IN ELMY H-MODE REGIMES

The plasmas shown in Table I demonstrate net progress towards the ITER targets, together with encouraging developments in ELM scaling. Extensions of ELMy H-mode studies to plasmas with higher currents, fields and heating powers and longer flat-top duration are planned. Plasmas with higher absolute densities and nearer to ρ^*_{ITER} can be developed, testing the limits of high performance regimes, enabling studies of Type I ELM scaling at low, ITER-like, collisionality, and of NTM scaling. New plasma configurations with ITER values of κ and δ have already been developed and tested with current up to 2.5 MA. The estimated disruptive force implies that such plasmas can be explored, up to 4MA/4T, when more auxiliary power becomes available. NTM control techniques will be tested. Work on Type II ELM regimes will continue.

3. ADVANCED TOKAMAK RESEARCH ON JET

The ultimate goal of Advanced Tokamak (AT) research is to provide steady-state operational regimes with possibly improved fusion performance. These modes are candidate for the steady-state operation of ITER [1]. Presently, AT research on JET is mainly focused on plasmas with internal transport barriers (ITBs) [7, 51]. In Section 3.1 experimental and modelling progress in ITB physics is reported. In Section 3.2 the achievement of high performance and of long pulse ITB plasmas is presented. The demonstration of real-time control of pressure and current profiles is reported in Section 3.3.

3.1. INTERNAL TRANSPORT BARRIER PHYSICS

3.1.1. A novel criterion for characterisation of ITBs

Barrier formation and strength are operationally characterised in JET by $\rho^*_T = \rho_s/L_T$ (ρ_s: ion Larmor radius, at the ion sound speed, L_T: local T_e gradient length). Analysis of the JET ITB database and of a set of turbulence simulations led to the ITB onset criterion $\rho^*_T > 0.014$ [13, 52]. ρ^*_T can be computed in real time, characterising ITB formation and evolution (see Figure 6), and providing an input for real time control (Section 3.2). Obviously this criterion does not capture the special role of rational q surfaces and magnetic shear, on which we comment below (Section 3.1.4).

3.1.2. LHCD aids current profile shaping

Coupling of the Lower Hybrid wave in all type of plasmas was greatly improved by puffing CD_4 near the launcher and matching the plasma shape [53, 54, 55]. Further optimisation led to a dramatic increase in the availability of the LH system, with power levels in the 3–4 MW range routinely coupled to high power 15–20 MW plasmas. Lower Hybrid Current Drive (LHCD) became an efficient tool to access ITBs and control them through off-axis current drive. Off-axis co-LHCD in the prelude phase (current ramp up) of JET plasmas easily and reliably provides magnetic shear reversal, providing target plasmas with appropriate current profile often exhibiting an early 'electron barrier'. The current profile is then 'frozen' by the application of heating (NBI, ICRH) and ITBs develop.

3.1.3. Current holes

Motional Stark effect measurements (MSE) of the poloidal magnetic field [56] showed plasmas with essentially no toroidal current density in the core of JET ITB discharges (a region of up to 20 cm diameter). These where explained as an effect of the non-inductive, off-axis co-LHCD, which induces a negative voltage in the plasma core. Similar 'current holes' were observed in JT-60 but driven solely by NBCD and bootstrap [57, 58]. The core current density does not appear to become negative (error bars on plasma core current are ±10–20 kA), although current diffusion calculations indicate that there is sufficient core negative voltage to cause current reversal [59]. This apparent clamping of the core current density near zero is consistent with n = 0 reconnection events redistributing the core current soon after it goes negative, as shown in reduced resistive MHD simulations in cylindrical geometry [60] and in 2-D nonlinear resistive MHD simulations in toroidal geometry [61].

3.1.4. Rational q surfaces and transport barrier trigger

Analysis of both low shear and reversed shear ITBs demonstrates the key role played by the q-profile itself and, in particular, by the presence of q = 1, 2 or 3 surfaces in the plasma edge and core [14]. The formation of low shear ITBs is well correlated with the occurrence of rational edge-q values. A model of coupled magnetic islands does show that a significant amount of rotational shear can be generated around $q_{min} = 2$ with an edge magnetic perturbation in agreement with measurements [62]. With reversed magnetic shear, experimental evidence also suggests a link between the appearance/development of an ITB and rational *q* surfaces (e.g. $q_{min} = 2$) entering the plasma core [63], as shown in Figure 6. Note that the effect of integer q value as an ITB trigger is only evident when marginal heating power is applied: with sufficient power, barrier formation can be independent of the q profile. Possible explanations for the influence of q on ITB formation are put forward: coupling of MHD modes located at rational q surfaces can generate stabilising velocity shear and gaps in the density of rational surfaces near rational q surfaces can have a stabilising effect on low wave number ITG/TEM turbulence [13, 14]. Simulations of ITG/TEM turbulence support this second explanation, showing that a barrier is more easily triggered when q_{min} is close to a low order rational surface provided the magnetic shear is low enough. The coexistence of two barriers located on a double q = 2 surface is also demonstrated.

ITG/TEM simulations of ITB plasmas successfully reproduce the amplification of a cold pulse at the outer edge of the barrier, as observed in JET when launching a shallow pellet or injecting impurities [12]. Cold pulses are damped inside the ITB region, as expected in a region with low diffusivity.

3.1.5. Alfvén cascades

In JET reversed shear ITB plasmas, cascades of Alfvén modes sweeping upwards in frequency have been observed [64], similar to observations in JT60-U [65]. Each cascade consists of many

modes, driven by ICRF-accelerated ions. These Alfvén cascades have been interpreted in terms of a novel-type of Energetic Particle Mode [66, 67, 68] localised at the point where $q(r)$ has a minimum. The frequency of the Eigenmode tracks the evolution of q_{min}, which opens the possibility of Alfvén spectroscopy measurement of q(r, t) [69]. Indeed Alfvén cascades are now used as an auxiliary rational q measurement on JET, as well as identifiers of shear reversal. 'Grand-cascades', sets of various TAE modes with (m, n) values corresponding to integer q_{min}, can be used to diagnose the q_{min} value as a function of time. The intrinsic interest of TAEs and cascades in potential steady state burning plasmas is being explored by various groups [10, 38, 70].

3.2. HIGH PERFORMANCE AND STEADY STATE ITBS

Advanced Tokamak scenarios have been extended in two directions: improved confinement and steady state. The ultimate objective is to combine both, together with appropriate density.

3.2.1. High performance ITBs

In transient states, reversed shear high performance plasmas with wide ITBs (r/a ~ 0.6) have been achieved. The stronger ITBs are triggered when q_{min} reaches 2, and within experimental uncertainties, ITBs are detected simultaneously, and at the same location, in electron and ion temperatures (T_e and T_i), density and plasma rotation profiles.

With reversed magnetic shear, the access power is low, and β_N and the fusion yield for given input power is high. The parameters of one of the highest performance ITB plasmas are shown in Table II [71]. Notably $\beta_N = 2.4$, and $q_{95} = 4.9$, with 2.5 MA of plasma current. The current profile is broad, maximum available heating (4MW ICRH and 17MW NBI) was used. Density peaking leads to impurity accumulation [15]. In this case, the transient high performance phase ends with a large ELM followed by a disruption. (global pressure n = 1 kink mode instability).

3.2.2. Record long pulse ITBs

By tailoring the internal plasma profiles to keep confinement and stability under control, the duration of ion ITBs could be prolonged to up to 7.5 seconds of plasma flattop, corresponding to $27 \times \tau_E$ [7, 72, 73]. The discharge parameters are presented in Table II. This is a record duration for an ion ITB in JET. In this case, an electron ITB was formed during the ramp-up, and had an overall duration of $37 \times \tau_E$. In this long duration ITB discharge, the fusion performance is lower than in transient cases (see Table II), while the non-inductive current fraction was much larger. Radiative or MHD core collapses of the ITB are observed: plasma pressure, toroidal rotation and electric fields collapse on a fast time scale. Surprisingly, the ITB is reformed immediately after the collapses. The implication, supported by turbulence simulation studies, is that as long as the q profile is not affected by the collapses, it remains favourable for ITB formation, and the ITB will re-form. At a slightly lower plasma current of 1.8 MA full non-inductive current drive was realised, as shown in Figure 7.

Table II: Advanced Tokamak Scenario development on JET

JET ITBs and ITER Target	*High Performance (pulse 51976, t = 6.8s, Ip = 2.5MA, Bt =3.45T)*	*Long pulse (pulse 53521, t = 10s, Ip = 2.0MA, Bt = 3.45T)*	*ITER Target as derived from ITER design basis [1]*
$H_{H\ (IPB98y-2)(thermal)}$	1.9	1	> 1.5
$H_{\ ITER\ 89\ L-P}$	3.3	2.1	
β_N	2.4	1.7	> 3.0
$I_{Non-Inductive}/I_p$	55%	90%	100%
I_{boot}/I_p	40%	50%	> 60%
q_{95}	4.9	5.5	4.5
P_{rad}/P_{tot}	15%	23%	75%
n_{io}/n_{eo}	$0.7 = (3.85/5.5)\ 10^{19}$	$0.65 = (4/6.2)\ 10^{19}$	
$\tau/\tau_{conf.}$, $\tau/\tau_{resistive}$ (*)	2, ~0.1	27, ~1	
n_{eo}/n_{GW}, n_{el}/n_{GW}	0.65, 0.35	0.8, 0.5	$n_{el}/n_{GW} > 0.6$
Edge	Type III ELMs	Type III ELMs	Mild ELMs

* τ = duration of ITB regime; $\tau_{resistive}$ is calculated at the ITB foot-point.

3.2.3. Development of real time control tools

Achieving steady-state real-time control of ITBs requires diagnostics allowing a reliable characterisation of the key parameters and appropriate actuators. The new ITB criterion ρ^*_T is used to characterise ITBs in real time, interfero-polarimetry provides a q profile measurement and the neutron production rate characterises ITB plasma performance. All these real time measurements are used as input values for the new Real Time Control System. The main actuators used are the three heating systems, LHCD, NB and ICRH, all having different (but coupled) effects on ITB behaviour.

3.2.4. Demonstration: real time control of pressure and current profiles

The above-mentioned tools have been used in a first series of real time feedback demonstrations, based on the largely non-inductive long pulse discharges described above. Pressure profile and barrier strength control is illustrated in Figure 6. Having established an appropriate target current profile, reliable and reproducible ITB operation is achieved by controlling the neutron yield by NBI heating, while ICRH is used to act on the maximum electron temperature gradient directly [74]. The LHCD is maintained in a pre-programmed way to provide a broad q-profile ensuring core confinement and stability. During the control phase, the plasma parameters of the discharge are fairly stationary with mild and continuous ELM activity. Thanks to the real time control of the ITB characteristics, the improved confinement state is maintained in a reproducible and stationary manner, e.g. avoiding the occurrence of core collapses. In separate experiments, it has also been shown that the LHCD feedback can be used in conjunction with real time measurement of q to maintain a desired q profile fixed for several seconds [75]. These demonstrations open the path toward fully controlled steady state Advanced Tokamak plasmas.

3.3. THE FUTURE: HIGH PERFORMANCE IN STEADY STATE

The plasmas shown in Table II demonstrate net progress towards the ITER target of steady state plasmas. To achieve steady-state high fusion performance, the current and pressure profile must be controlled simultaneously, the density must approach the Greenwald value, impurity accumulation must be avoided or controlled, bootstrap must be high (high pressure and high power), and edge radiation must be increased, or the SOL broadened. Operation in ITER-like triangularity, made possible by the recent divertor modification, contributes to make the results more directly applicable to ITER prediction.

4. PHYSICS STUDIES IN VARIOUS OPERATING REGIMES.

We present here some important physics studies that do not necessarily focus on ELMy H-mode or ITB plasmas.

4.1. DIAGNOSTIC DEVELOPMENTS

4.1.1. Gamma rays

Nuclear reaction γ-ray diagnosis has proven its value for studying fast ions in JET [37]. Intense γ-ray emission is produced when fast ions (ICRF-driven ions, fusion products, NBI-injected ions) react either with fuel ions or with the plasma impurities such as carbon and beryllium. Analysis of γ-ray spectra led to the identification, in different experiments, of several nuclear reactions involving fast particles accelerated by ICRF and plasma ions. The reaction $^{9}Be(\alpha, n\gamma)^{12}C$, proposed as a fusion γ-particle diagnostic led to identification of tail α-particle with energies in excess of 2 MeV, as described in Section 2.2.2. Identification of RF induced orbit pinch was possible with this diagnostic (see Section 4.2.2).

4.1.2. Non-Maxwellian bulk electron distribution measurements

Evidence of non-Maxwellian bulk electron distribution functions was found on FTU [76] in low-shear plasmas with central ECRH (~ 0.8 MW), and in JET [77, 78] in regimes with high levels of ICRF and NBI power (Hot Ion H-mode). An analysis of the various harmonics of electron cyclotron emission spectra (ECE) has been carried out, based on extensive modelling. The distorted distribution function obtained from the ECE data can explain the discrepancy between the Thomson scattering (TS) and ECE measurements of electron temperature (T_e). Such discrepancies between ECE and TS temperatures have also been observed in regimes with alpha heating on both TFTR [79] and JET [80], making the understanding of this phenomenon and of its implications an important fusion issue.

4.2. ICRF STUDIES

As well as supporting a variety of other experiments, the ICRH system in JET was used for some specific experiments briefly described here.

4.2.1. Rotation

In future fusion devices, external momentum input will be much lower than in most present- day tokamaks. Rotation is known to increase the stabilising effect of a resistive wall, as is rotation shear in improved confinement regimes. For extrapolation to next step devices, it is important to study these issues in plasmas with lower momentum input. The toroidal rotation of ICRF-only heated plasmas has been investigated in the JET tokamak. When the minority cyclotron resonance layer is far off-axis, the toroidal rotation profiles are hollow, and dominantly co-current [81, 82, 83]. In contrast to the predictions of theories that rely mainly on effects arising from ICRF-driven fast ions to account for ICRF-induced plasma rotation, there is only a slight difference between a high field side or a low field side position of this resonance layer. A more central deposition of the ICRF power in L-mode and operation in H-mode both leads to more centrally peaked profiles, both in the co-direction. The data provides a basis for theory development.

4.2.2. Pinch of fast particles

Theory predicts that ICRF waves with a directed spectrum will influence the radial transport of the minority particles with which they interact. Waves with a co-directed spectrum lead to an inward pinch of the energetic particles, and waves with a counter-directed spectrum to an outward pinch of those particles. Recent advances [37] in the tomographic reconstruction of the measured γ-ray emission data provide direct experimental evidence of this effect. This result [84], together with concurrent experimental evidence from Alfvén eigenmodes, sawtooth periods, electron temperatures and fast ion energies, shows that the ICRF-induced pinch provides a tool to affect the radial fast ion profile and the plasma heating profile.

4.3. TRANSIENT HEAT TRANSPORT STUDIES, COLD PULSES

Heat pulse propagation studies were carried out in JET, using ICRF mode conversion heating (^{3}He in D and ^{4}He) [85] as a localised source of electron heating. Results of the transport analysis [12] are consistent with the existence of a threshold of the inverse critical electron temperature gradient length and a 'medium' level of stiffness in the electron channel, as discussed in Section 2.3.5.

On the other hand, cold pulse propagation experiments, in L-mode and ITB plasmas, show fast propagation from edge to core, which can not be explained by stiffness alone: non-local models must be considered [12].

4.4. DISRUPTION STUDIES

4.4.1. Thermal loads

The current ITER assumption for disruptions is that the energy from the thermal quench is deposited in the divertor. Recent analysis shows that only a few percent of the thermal and thermal plus magnetic energy can be accounted for in the JET divertor [86] and it is spread rather uniformly. If

the same applies in ITER, then the energy density within the divertor would be below the level at which carbon ablation or tungsten melt layer formation are expected [3].

4.4.2. VDEs, Neutral Point

Modelling of vertical displacement events (VDEs) in JET has improved, with a better representation of eddy currents in the vacuum vessel now incorporated in the simulation codes. There is good agreement between theoretical predictions of VDE evolution and experimental results: growth rates have been estimated within an accuracy of 5% for plasmas with a growth time longer than 2 ms [87, 88]. The Neutral Point has been identified in dedicated experiments on JET [89], confirmed with simulations done with the linearised equilibrium code CREATE-L [87]. It has been observed that a plasma, specially designed to be set at different vertical equilibrium position without altering its shape, moves upwards (downwards) when the disruption is triggered by argon puffing with the plasma below (above) the Neutral Point.

4.4.3. Runaways

Regions of parameter space have been identified in which disruptions lead to runaway generation in JET [90]. They appear when q_{95} and B_t exceed threshold values (i.e. B_t above ~2T), in good agreement with observations on JT60-U [91]. The delay in runaway generation following the temperature collapse is found to be caused by the very high density generated by the disruption. It can be concluded that avalanching is probably the dominant process in runaway electron formation in JET and therefore runaway control techniques can be tested for ITER. Initial tests in this regime have shown that it is possible to quench the plasma with large helium puffs without producing runaways.

4.4.4. Halo currents

The JET halo current diagnostics have been refurbished [92] with measurements of the poloidal halo current now available in three locations, 90˚ apart, at the top of the vessel. The old system had at most 2 locations 180˚ apart available at the top of the vessel. The toroidal peaking factor (ratio of the largest to the toroidally averaged halo current) can now be determined with improved certainty.

The data collected in the past year of operation, which include dedicated disruption experiments, indicate that the maximum halo fraction is < 30% and the maximum toroidal peaking factor is < 2. This is in reasonable agreement with what was observed using the old set of probes and maintains the JET data below the envelope used for the design of ITER [1]. Thus, the improved JET data continues to validate the ITER design assumptions.

5. EROSION AND CO-DEPOSITION

Erosion and deposition constitute one of the key topics in preparation of ITER operation, as they influence the lifetime of divertor tiles and other plasma facing components (PFCs), and the in-vessel tritium inventory. JET experiments provide a database against which models can be tested [16].

Tiles from the MkII-GB divertor were removed during the 2001 shutdown. Analysis of tile surfaces [93, 94] confirmed previous observations: the inner divertor is subject to net deposition of plasma impurities (and retention of D and T). No comparable net erosion is observed in the outer divertor, implying that the primary source of eroded impurities are main chamber PFCs. This analysis shows that deposited films are enriched in Be and other metals, while carbon is chemically eroded and transported to shadowed regions of the inner divertor [95].

Measurements made during the 2001 He campaign differentiate physical and chemical sputtering. The main source of C in L-mode plasmas appears to be chemical sputtering at the inner divertor and main chamber wall. In ELMy H-mode the situation is less clear, but the data points to a strong physically sputtered C-source from the main chamber and outer divertor [96], while chemical erosion dominates in the inner divertor in all cases.

In ohmic plasmas, atoms of ^{13}C were injected into the top of the JET vessel, at the end of the MarkIIGB operation (divertor temperature had been lowered to ~100˚C). About one-half of the injected ^{13}C is found on the inner divertor tiles intersected by the SOL, and a negligible amount is found at the outer divertor [93], consistent with previous findings. No ^{13}C was found on shadowed regions of the tiles, where otherwise thick carbon layers have built up in the past [95]. This may indicate a reduced long range carbon transport due to reduced chemical erosion at lower operating temperatures [94], but it might be also connected with the special (ohmic) plasma operating conditions [16].

First measurements of pulse resolved growth of carbon layers near the inner louver situated inside the divertor pumping throat have been made with a newly developed quartz micro-balance. This diagnostic is capable of measuring deposited layers at the mono-atomic layer level. The average growth rate (deposited carbon atom on louver divided by total ion flux into the inner divertor) was found to be of order $2\ 10^{-4}$ C/ion [97], 200 times smaller than previously estimated from the DT campaign. A thorough investigation is underway to explain these differences.

6. TRITIUM TECHNOLOGY R&D

Special detritiation techniques are developed for components replaced during operations to allow waste disposal under economically sound and environmentally safe conditions [98, 99, 100]. Water detritiation techniques are also being developed: laboratory size plants with liquid phase catalytic exchange (LPCE) column have been built to test the performance of various packing materials and catalysts and to determine mass transfer for D and T between water and gas [101,102]. Design studies of a water detritiation plant at JET are on going [103]. During the 2001 shutdown flakes from the sub-divertor region of the tokamak were collected remotely to help reconcile the tritium balance at JET [104, 105], as described in Section 5.

7. FUTURE PLANS

The present plan of exploitation of the JET facilities for the years 2003 and 2004 foresees experimental campaigns in 2003 and until February 2004. In 2003, the following experiments are planned:

development of ELMy H-mode and ITB modes, Trace Tritium Experiments in deuterium plasmas, reversed magnetic field experiments in deuterium. The last campaigns before the 2004 shutdown are reserved for hydrogen and helium plasmas: they will provide data in preparation of ITER's non-activation phase. From March 2004 a long shut down period is planned for installation of enhancements.

The Trace Tritium Experiment (TTE) shall take full advantage of the unique Tritium handling capability of JET. The TTE is planned with ~1.5% Tritium in Deuterium plasmas. Transport of Tritium particles will be investigated with neutron and γ emission diagnostics. A study of particle (fuel ion, Helium and impurities) transport is planned in ELMy H-modes and AT scenarios, continuing and greatly extending the work initiated in the previous Trace Tritium Experiment [106]. In particular, a study of fuel ion transport has never been done in AT scenarios, and would be important in preparation of future DT AT operation on JET or/and ITER. The use of trace tritium also offers an opportunity to study aspects of ICRF heating schemes and Fast Particle Physics (fast ions in current hole scenarios). The TTE has the added benefit of exercising and maintaining technical expertise on tritium handling in a tokamak environment. It finally permits relevant testing of new systems foreseen to find application on ITER, such as detritiation catalysts, and an ITER-design cryo-panel [107, 108].

In the 2004 shutdown it is planned to install a new in-port ICRF antenna. The aims are to validate key elements of the ITER ICRF design (such as ELM-tolerant operation at high power density), and to deliver an additional 7 MW of heating power, allowing higher performance operation closer to ITER plasma parameters. By then, planned diagnostic upgrades include CXRS core and edge, magnetics, bolometry, neutron spectrometry, microwave waveguides, divertor diagnostics. New diagnostics to be installed include a high resolution Thomson Scattering System, TAE active antenna system, wide angle Infra-Red view, Halo Sensors, Lost α detectors and a comprehensive system of erosion/re-deposition diagnostics.

8. CONCLUSIONS

JET continues to provide vital contributions to understanding of tokamak physics, scaling predictions for ITER, further development of ITER operating scenarios and testing of ITER relevant systems, such as heating and current drive, diagnostics and Tritium technologies.

ACKNOWLEDGEMENTS

This work was performed under EFDA, by the JET EFDA contributors, listed in Annex I. Special contributions to this paper were made by M. Bécoulet, D. Brennan, F. Crisanti, S. Ciattaglia, P. Coad, X. Garbet, T.T.C. Jones, E. Joffrin, N. Hawkes, T. Hender, G. Huysmans, V. Krivenski, X. Litaudon, P.J. Lomas, A. Loarte, D. McDonald, P. Mantica, M. Mantsinen, G. Matthews, P. Monier-Garbet, D. Moreau, F. Nave, J.-M. Noterdaeme, J. Ongena, S. Pinches, R. Pitts, V. Philipps, J. Rapp, V. Riccardo, G. Saibene, J. Sanchez, R. Sartori, O. Sauter, D. Stork, B. Stratton, D. Testa, A. Tuccillo, M. Valovic, S. Sharapov, H. Weisen and K.-D. Zastrow. The dedication and hard work of

the UKAEA colleagues responsible for JET operation is gratefully acknowledged. We dedicate this article to the memory of Derek C. Robinson, FRS, who contributed greatly to fusion development for four decades.

REFERENCES

[1] ITER Physics Basis, Nucl. Fusion, **29** (1999) 2368.

[2] Loarte, A., 'Type I ELM energy and particle losses in JET ELMy H-modes and implications for ITER', these proceedings (paper EX/P1-08).

[3] Matthews, G.F., 'Steady state and transient power loads in JET', these proceedings (paper EX/D1-1).

[4] Rapp, J., 'Reduction of divertor heat load in JET ELMy H-modes using impurity seeding techniques', these proceedings (paper EX/P1-09).

[5] Parail, V., 'Integrated Modelling of JET H-mode Plasmas with type-I ELMs', these proceedings (paper TH/P3-08).

[6] Koslowski, H.R., 'Observation of Pre- and Postcursor Modes of Types I ELMs on JET', these proceedings (paper EX/P1-14).

[7] Litaudon, X., 'Progress towards steady state operation and real time control of internal transport barriers in JET', these proceedings (paper EX/C3-4).

[8] Hender, T., 'Sawtooth, Neo-Classical Tearing Mode and Error Field Studies in JET', these proceedings (paper EX/S1-2).

[9] Ongena, J., 'Towards the realization on JET of an integrated H-Mode scenario for ITER', these proceedings (paper EX/C2-4).

[10] Testa, D., 'Experimental Study of the Stability of Alfven Eigenmodes on JET', these proceedings (paper EX/P1-17).

[11] Noterdaeme, J.-M., 'Heating, current drive and energetic particles studies on JET in preparation of ITER operation', these proceedings (paper EX/W-1).

[12] Mantica, P., 'Transient Heat Transport Studies in JET Conventional and Advanced Tokamak Plasmas', these proceedings (paper EX/P1-04).

[13] Garbet, X., 'Micro-stability and Transport Studies of Internal Barriers in JET', these proceedings (paper TH/2-1).

[14] Joffrin, E., 'Internal Transport Barrier triggering by rational magnetic flux surfaces', these proceedings (paper EX/P1-13).

[15] Dux, R., 'Impurity transport in internal barrier discharges on JET', these proceedings (paper EX/C3-5Ra).

[16] Philipps, V., 'Recent results on long term fuel retention in JET and TEXTOR and predictions for ITER', these proceedings (paper EX/P5-08).

[17] Suttrop, W., 'Parameter similarity studies in JET, ASDEX Upgrade and ALCATOR C-Mod', these proceedings (paper EX/P5-07).

[18] Hidalgo, C., 'Experimental evidence of fluctuations and flows near marginal stability in the plasma boundary region in fusion plasmas', these proceedings (paper EX/C4-4).
[19] Castaldo, C., *et. al.*, 'Transport barriers produced in JET discharges by ion Bernstein waves', post-deadline paper, these proceedings.
[20] Special issue on 'ELMy H-Mode Research on the JET Facility under EFDA during the 2000-2001 Experimental Campaign', Plasma Phys. Control. Fusion **44** No.9 (2002).
[21] Suttrop, W., Phys. Plasmas, **9** (2002) 2103.
[22] Loarte, A., *et al*., *ibid*., PPCF, 44, No.9, p.1815-1844.
[23] Saibene, G., *ibid*., PPCF, 44, No.9, p.1769-1799.
[24] Janeschitz, G., *et al*., Jour. Nucl. Mat. **290-293** (2001) 1.
[25] Federici, G., *et al*., Proc. of 15th Int. Conf. on Plasma Surface Interactions in Controlled Fusion Devices, May 27-31, 2002, Gifu, Japan, to be published in JNM.
[26] Huysmans, G.T.A., 'Overview of MHD stability in edge transport barriers', presented at the 9th European Fusion Physics Workshop 2001, Saariselka, Finland, 2001.
[27] Huysmans, G.T.A., *et al*., Phys. Plasmas **8** (2001) 4292.
[28] Perez, C., *et al*., 'Type-I ELM Precursor Modes in JET', submitted to Nucl. Fusion.
[29] Söldner, F.X., *et al*., Plasma Phys. Control. Fusion **39** (1997) B353.
[30] Bécoulet, M., *et al*., Plasma Phys. Control. Fusion **44** 2002 A103.
[31] Nave, M.F.F., *et al.*, Nucl. Fusion **42** (2002) 2.
[32] Guenter, S., *et al*., Phys. Rev. Lett. **8**7, 275001 (2001).
[33] Sauter, O., *et al*., Phys. Rev. Lett., **88** (2002) 105001.
[34] Lahaye, R.J., Phys. Plasmas **7**, 3349 (2000).
[35] Sauter, O., Plasma Phys. Control. Fusion **44** (2002), p. 1999.
[36] Mantsinen, M., *et al*., Phys. Rev. Letters **88** (2002) 105002-1.
[37] Kiptily, V.G., *et al.*, Nucl.Fusion **42** (2002) 999.
[38] Jaun, A., *et al*., 'Collective modes and Fast Particle Confinement in ITER', these proceedings, (paper CT/P-06).
[39] Sartori, *et al*., Plasma Phys. Control. Fusion **44** (2002) 1801.
[40] Stober, J., *et al*., Nucl. Fusion **41** (2001) 1123.
[41] Kamada, Y., and the JT60-U team, Nucl. Fusion **41** (2001) 1311.
[42] Nave, F., *et al*., 'Control of Impurity Accumulation in JET Radiative Mantle Discharges', submitted to Nucl. Fusion.
[43] Lang, P.T., *et al*., Nucl. Fusion **42** (2002) 388.
[44] Valovic, M., *et al*., Plasma Phys. Control. Fusion **44** (2002) 1911.
[45] Garzotti, L., *et al*., 'Particle Transport and Density Profile Analysis of Different JET Plasmas', 29th EPS Conference on Plasma Phys. and Contr. Fusion Montreux, 17-21 June 2002 ECA Vol. 26B, P-1.035 (2002).
[46] Cordey, G., Plasma Phys. Control. Fusion, **44** (2002) 1929.

[47] McDonald, D., in preparation.
[48] Wolf, R.C., *et al*., 'Characterisation of ion heat conduction in JET and ASDEX-Upgrade plasmas with and without internal transport barriers', submitted to Plasma Physics and Controlled Fusion.
[49] Jones, T.T.C., Bickley, A.J., Felton, R., *et al*., 'Simulation of Alpha Particle Plasma Self-Heating Using ICRH Under Real-Time Control', 28th EPS Conference on Plasma Phys. and Contr. Fusion, Madeira, 2001, ECA Vol. **25A** (2001) 1197-1200.
[50] Tuccillo, A.A., Baranov, Y., Barbato, E., *et al*., Proc. 14th Topical Conference on Radiofrequency Power in Plasmas, Oxnard 2001, (Eds.) T.K. Mau, J. deGrassie, AIP Conference Proceedings **595**, 209-216 (2001).
[51] Special issue on *'Advanced tokamak research in EFDA-JET during the 2000-2001 experimental campaigns'* 2002 Plasma Phys. Control. Fusion **44** 1031.
[52] Tresset, G., *et al*., Nucl. Fusion **42** (2002) 520.
[53] Mailloux, J., *et al*., Phys. Plasmas **9** (2002) 2156.
[54] Pericoli, V., *et al*., *Radio Frequency Power in Plasmas,* (14th Topical Conf., Oxnard, CA, 2001), Vol. 595, AIP (2001) 245-248, submitted to Phys. of Plasmas.
[55] Pericoli, V., *et al.*, 'Study and optimisation of lower hybrid waves coupling in advanced scenarios plasmas in JET', submitted to Physics of Plasmas (2002).
[56] Hawkes, N.C., *et al*., Phys. Rev. Lett. **87** (2001) 115001-1.
[57] Fujita, T., Phys. Rev. Lett. **87** (2001) 245001.
[58] Miura, Y., these proceedings (paper EX/C3-1Ra).
[59] Tala, T.J.J., *et al*., Plasma Phys. Control. Fusion **43** (2001) 507.
[60] Huysmans, G.T.A., *et al*., Phys. Rev. Lett. **87** (2001) 245002-1.
[61] Stratton, B.C., *et al*., Plasma Phys. Control. Fusion **44** (2002) 1127.
[62] Joffrin, E., *et al*., Nucl. Fusion **42** (2002) 235.
[63] Joffrin, E., *et al*., Plasma Phys. Control. Fusion **44** (2002) 1739.
[64] Sharapov, S.E., *et al*., Phys. Lett. A 289 (2001) 127.
[65] Kimura, H., *et al*., Nuclear Fusion **38** (1998)1303.
[66] Sharapov, S.E., *et al*., Phys. Plasmas 9, 2027 (2002).
[67] Zonca, F., 'Energetic Particle Mode Stability in Tokamaks with Hollow q-profiles', to be published in Phys. Plas.
[68] Berk, H.L., *et al.,* Phys. Rev. Lett. **87** (2001) 185002.
[69] Fasoli, A., *et. al*., PPCF, to appear 2002.
[70] Breizman, B.N., *et al.*, 'Alfvén Eigenmodes in Shear Reversed Plasmas', these proceedings (paper TH/4-3).
[71] Challis, C.D., *et al.*, Plasma Phys. Control. Fusion **44** (2002) 1031.
[72] Crisanti, F., *et al*., Phys. Rev. Lett. **88** (2002) 145004-1.
[73] Litaudon, X., *et al*., Plasma Phys. Control. Fusion **44** (2002) 1057.
[74] Mazon, D., *et al*., Plasma Phys. Control. Fusion **44** (2002) 1087.

[75] Mazon, D., *et al*., Proc. of 29th Eur. Phys. Conf., Montreux (EPS).
[76] Krivenski, V., submitted for publication.
[77] Krivenski, V., *et al*., 29th EPS Conference on Plasma Phys. and Contr. Fusion, Montreux, 2002, ECA **26B**, O-1.03 (2002).
[78] De La Luna, E., *et al*., 14th Topical Conference on High Temperature Plasma Diagnostics, Madison, 2002.
[79] Taylor, G., *et al*., Phys. Rev. Lett. (1996).
[80] Thomas, P.R., *et al*., Phys. Rev. Lett. **80**, 5548 (1998).
[81] Noterdaeme, J.-M., Righi, E., *et al*., 'Spatially resolved plasma rotation profiles with ICRF on JET', *Radio Frequency Power in Plasmas,* (14th Topical Conf., Oxnard, CA, 2001), Vol. 595, AIP (2001) 98-101.
[82] Noterdaeme, J.-M., Righi, E., *et al*., 'Toroidal plasma rotation with ICRF on JET', *Controlled Fusion and Plasma Physics,* (28th EPS Conf., Funchal (Madeira), Portugal, 2001), Vol. ECA 25A, EPS (2001) 777-780.
[83] Noterdaeme, J.-M., Righi, E., *et al*., 'Spatially resolved plasma rotation profiles with ICRF on JET', subm. to Nucl. Fusion (2002).
[84] Mantsinen, M., Ingesson, L.C., *et al*., 'Controlling the profile of ion-cyclotron-resonant ions in JET with the wave-induced pinch effect', Phys. Rev. Letters **89** (2002) 115004-1-115004-4.
[85] Mantsinen, M., Mayoral, M.-L., *et al*., 'ICRF Mode Conversion Experiments on JET', Controlled Fusion and Plasma Physics, (28th EPS Conf., Funchal (Madeira), Portugal, 2001), Vol. ECA 25A, EPS (2001) 1745-1748.
[86] Riccardo, V., *et al*., Plasma Phys. Contr. Fusion **44** (2002) 905-929.
[87] Albanese, R., *et al*., Nucl. Fusion, **38** (1998) 723.
[88] Albanese, R., *et al.*, submitted to Nucl. Fus., 2002.
[89] Villone, F., *et al*., 'Neutral Point Detection In JET', Proc. of 22nd Symposium on Fusion Technology (SOFT), Helsinki, Sept. 2002, to be published in Fusion Eng. and Design.
[90] Gill, R.D., *et al.*, 'Behaviour of disruption generated runaways in JET', accepted for publication in Nuclear Fusion (2002).
[91] Yoshino, R., *et al*., Nuclear Fusion **39** (1999) 151.
[92] Riccardo, V., *et al*., 'Refurbishment of the JET halo current diagnostics', Proc. of 22nd Symposium on Fusion Technology (SOFT), Helsinki, Sept. 2002, to be published in Fusion Eng. and Design.
[93] Likkonen, J., *et al*., Proc. of 22nd Symposium on Fusion Technology (SOFT), Helsinki, Sept. 2002.
[94] Coad, J.P., *et al.*, Proc. of 15th PSI, Gifu, Japan, to be published in J. Nucl. Materials.
[95] Coad, J.P., *et al*., J Nucl. Materials 290-293 (2001) 224.
[96] Pitts, R., *et al.*, *ibid*., 15th PSI, Gifu, 2002, to be published in J. Nucl. Materials.
[97] Esser, H.G., *ibid*., 22nd SOFT, Helsinki, 2002.

[98] Bell, A.C., *et al*., Fusion Science and Technology **41** (2002) 626.
[99] Rosanvallon, S., *et al*., Fusion Science and Technology **41** (2002) 695.
[100] Perevezentsev, A., *et al*., Fusion Science and Technology **41** (2002) 706.
[101] Cristescu, I., *et al*., 'Simultaneous tritium and deuterium transfer in a water detritiation CECE Facility at TLK', Proc. 22nd SOFT, Helsinki, Sept. 2002.
[102] Perevezentsev, A., *et al*., Fusion Science and Technology **41** (2002) 1107.
[103] Perevezentsev, A., *et al*., Fusion Eng. Design **00** (2002) 1-5.
[104] Perevezentsev, A., *et al*., Fusion Science and Technology **41** (2002) 821.
[105] Coad, J.P., *et al*., J. Nucl. Materials **290-293** (2002) 224.
[106] JET TEAM, presented by Zastrow, K.-D., Nucl Fus **39** (1999) 1891.
[107] Brennan, D.P., Fusion Science and Technology, **41** (2002) 578.
[108] Day, CHR., *et al*., 'A large scale cryopanel test arrangement for tritium pumping', Proc. 22nd SOFT, Helsinki, Sept. 2002.

ANNEX 1: JET EFDA CONTRIBUTORS

J.M. Adams[15], G. Agarici[15], M. Agarici[2], H. Akhter[15], R. Albanese[5,c], S. Alberti[12], S. Allfrey[12], B. Alper[15], D. Alves[9], J. Amarante[17], F.V. Amerongen[6], P. Andrew[15], Y. Andrew[15], J.M. Ane[2], C. Angioni[12], C. Antonucci[1, 5g], G. Apruzzese[5,b], G. Artaserse[5,c], J.F. Artaud[2], E. Ascasibar[3], E. Asp[10], M. Axton[15], A. Baciero[3], M. Badarelli[5,b], W. Baity[29], R. Balbin[3], S. Balme[2], O. Barana[5, a], Y. Baranov[15], E. Barbato[5, b], R. Barnsley[15], V. Basiuk[2], G. Bateman[27], S. B‰umel[8], P. Bayetti[2], L. Baylor[29], B. Beaumont[2], P. Beaumont[15], A. Bécoulet[2], M. Bécoulet2, M. Bekris[14], M. Beldishevski[15], A.C. Bell[15], P. Bennet[15], G. Berger-By[2], H.L. Berk[25], S. Bernabei[30], L. Bertalot[5,b], B. Bertrand[2], M. Beurskens[15], M. Beurskens[6], ??. Bibet[2], A. Bickley[15], M. Bigi[15], R. Bilato[8], T. Blackman[15], P. Blanchard[12], J. Blum[21], T. Bolzonella[5, a], A. Bondeson[10], W. Bongers[6], G. Bonheure[17], X. Bonnin[8], K. Borass[8], D. Borba[1, 9], K. Bosak[21], P. Bosia[2], H. Boyer[15], G. Bracco[5, b], G.C. Braithwaite[15], B.N. Breizman[25], S. Bremond[2], P.D. Brennan[15], J. Bresslau[30], S. Brezinsek[7], B. Brichero[17], F. Briscoe[15], M. Brix[7], G. Brolatti[5, b], D.P.D. Brown[15], A. Bruggeman[17], A. Bruschi[5, d], S. Bryan[15], J. Brzozowski[10], J. Bucalossi[2], G. Buceti[1, 5], M.A. Buckley[15], T. Budd[15], R. Budny[30], P. Buratti[5, b], P. Butcher[15], R.J. Buttery[15], G. CalabrÛ[5, c], C.J. CaldwelNichols[14], J. Callen[36], D. Campbell[16], D.C. Campling[15], B. Cannas[5, e], A.J. Capel[15], P.J. Card[15], T. Carlstrom[24], C. Castaldo[5, b], R. Causey[31], F.E. Cecil[23], R. Cesario[5, b], C. Challis[15], V. Chan[24], Ph. Chappuis[2], M. Charlet[15], JM. Charreau[2], C. Cheron[2], D. Child[15], G. Chitarin[5, a], S. Ciattaglia[1, 5], S. Cirant[5, d], D. Ciric[15], R. Clarke[15], J.P. Coad[15], P. Coates[15], V. Coccorese[5, c], V. Cocilovo[5, b], S. Coda[12], R. Coelho[9], I. Coffey[15], A. Coletti[5, b], S. Collins[15], J. Conboy[15], S. Conroy[10], G. Conway[8], S.R. Cooper[15], G. Cordey[15], Y. Corre[10], G. Corrigan[15], S. Cortes[9], D. Coster[8], G.F. Counsell[15], M. Cox[15], S.J. Cox[15], S. Cramp[15], C. Crescenzi[5, b], F. Crisanti[5, b], I. Cristescu[20], I.R. Cristescu[14], B. Crowley[4], N. Cruz[9], L. Cupido[9], R. Cusack[15], P. Da Silva Aresta Belo[9], S. Dailey[15], E. Daly[15], C. Damiani[1, 5f], D. Darrow[30], D. Darrow[15], O. David[2], N. Davies[15], C. Day[14], R. De Angelis[5, b], M. de Baar[15], O. De

Barbieri[16], M. De Benedetti[5, b], J. De Grassie[24], E. De la Luna[3], P. De Vries[6], F. Degli Agostini[5, a], M. Dentan[1, 2], A. Dimits[34], A. Dines[15], J.A. Dobbing[15], L. Doceul[2], J. Doncel[1,3], A. Donne[6], T. Donne[6], W. Dorland[22], S.E. Dorling[15], P. Doyle[15], V. Drozdov[15], O. Dumbrajs[13], P. Dumortier[17], A. Durocher[2], F. Durodié[17], B. Duval[12], R. Dux[8], T. Edlington[15], A.M. Edwards[15], D.C. Edwards[15], D.T. Edwards[15], P. Edwards[15], T. Eich[8], A. Ekedahl[2], D. Elbeze[2], B. Ellingboe[4], R. Ellis[30], C.G. Elsmore[15], B.S.Q. Elzendoorn[6], S.K. Erents[15], G. Ericsson[10], L. Eriksson[2], B. Esposito[5, b], H.G. Esser[7], T. Estrada[3], M. Evrard[17], C. Ewart[15], J. Fanthome[15], J.W. Farthing[15], D. Fasel[12], A. Fasoli[12], R. Felton[15], M. Fenstermacher[26], C. Fenzi[2], H. Fernandes[9], A. Fernandez[3], J. Ferreira[9], J.A. Fessey[15], A. Figueiredo[9], P. Finburg[15], J. Fink[8], K.H.. Finken[7], P. Fiorentin[5, a], U. Fischer[14], C. Fleming[15], R. Forrest[15], C. Fourment[2], B. Franel[2], P. Franzen[8], T. Fredian[28], J.P. Fricconneeu[2], D. Frigione[5, b], G. Fu[30], J.C. Fuchs[8], K. Fullard[15], W. Fundamenski[15], F. Gabriel[2], J. Gaffert[8], E. Galutschek[11], T. Gans[4], X. Garbet[2], I. GarciaCortes[3], L. Garzotti[5, a], E. Gauthier[2], J. Gedney[15], A. Geier[8], C. Gentile[30], S. Gerasimov[15], A. Geraud[2], P. Ghendrih[2], R. Giannella[2], R.D. Gill[15], C. Gimblett[15], E. Giovannozzi[5,b], C. Giroud[6], J. Goff[15], P. Gohil[24], A. Gondhalekar[15], M. Goniche[2], A. Goodyear[15], N. Gorelenkov[30], G. Gorini[5, d], R. Goulding[29], C.W. Gowers[15], M.E. Graham[15], L. Grando[5, a], G. Granucci[5, d], M. Graswinckel[6], N. Green[15], C. Greenfield[24], N. Greenough[30], M. Greenwald[28], D. Gregoratto[10], F.S. Griph[15], C. Grisolia[2], A. Grosman[2], G. Grosso[5, d], S. Gruenhagen[14], A. Gude[8], S. Guenter[8], K. Guenther[15], C. Guérin[2], M. Gugla[14], A. Guigon[1,2], R. Guirlet[2], J. Gunn[2], G. Haas[8], L. Hackett[15], S. Hacquin[9], T. S. Hahm[30], B. Haist[15], S. HallworthCook[15], D. Hamilton[15], G. Hammett[30], R. Handley[15], J.D.W. Harling[15], J. Harrison[15], D. Hartmann[8], T. Haupt[15], N.C. Hawkes[15], J. Hay[15], I. Hayward[15], J. Hedin[10], P. Heesterman[15], J. Heikkinen[13], B. Heinemann[8], P. Helander[15], P. Hellingman[6], T. Hellsten[1, 10], O.N. Hemming[15], R. Hemsworth[2], T.C. Hender[15], M. Henderson[12], P. Hennequin[2], A. Henshaw[15], A. Herrmann[8], C. Hidalgo[3], J. Hill[15], D. Hillis[29], M. Hitchin[15], T. Hoang[2], J. Hobirk[8], F. Hoekzema[7], J.A. Hoekzema[7], F. Hofmann[12], C. Hogan[29], C. Hogben[15], D. Hogeweij[6], D. Homfray[15], A. Horton[15], L.D. Horton[8], J. Hosea[30], A.J. Hoskins[15], S. Hotchin[15], M.R. Hough[15], W. Houlberg[29], J. How[2], D. Howell[15], M. Hron[18], A. Hubbard[28], A. Huber[7], Z. Hudson[15], H. Hume[15], D. Humphries[24], F. Hurd[16], I. Hutchinson[28], T. Hutter[2], S. Huygen[17], G. Huysmans[2], F. Imbeaux[2], C. Ingesson[6], P. Innocente[5, a], S. Jachmich[17], G. Jackson[24], S. Jardin[30], A. Jarmen[10], O.N. Jarvis[15], R. Jaspers[6], A. Jaun[10], I. Jenkins[15], H.S. Jensen[14], E. Joffrin[2], M.F. Johnson[15], R. Johnson[15], E.M. Jones[15], G. Jones[15], H.D. Jones[15], T. Jones[15], T. Jonsson[10], C. Jupen[10], A. Kallenbach[8], J. Kallne[10], S. Karttunen[13], W. Kasparek[14], A. Kaye[15], D. Keeling[15], D. Kelliher[4], N. Kemp[15], R.F. King[15], J. Kinsey[27], V. Kiptily[15], K. Kirov[8], A. Kirschner[7], T. Kiviniemi[13], P. Knight[15], S. Knipe[15], R. Koch[17], W. Kooijman[6], A. Korotkov[15], HR. Koslowski[7], G. Kramer[30], W. Kraus[8], A. Kritz[27], O.G. Kruijt[6], T. Kurki-Suonio[13], R.J. La Haye[24], B. Labombard[28], R. Laesser[14], N. Lam[15], Ph. Lamalle[1, 23], G. Land[6], P. Lang[8], L. Lao[24], J. Last[15], M. Laux[8], C. Laviron[2], K.D. Lawson[15], M. Laxaback[10], E. Lazzaro[5,d], H. Leggate[15], M. Lehnen[7], M. Leigheb[5, b], M. Lennholm[2], A. Leonard[24], C. Lescure[15], F. Leuterer[8], K. Likin[3], J. Likonen[13], K. Lingier[6], J. Linke[7], B. Lipshultz[28], J. Lister[12], X. Litaudon[2], Y. Liu[10], G. Lloyd[15], T. Loarer[2], A. Loarte[16], D. Loesser[30],

P.J. Lomas[15], F. Long[15], J. L^nnroth[13], A. Lorenz[1, 8], P. Lotte[2], F. Louche[17], M. Loughlin[15], A. Loving[15], T. Luce[24], R.M.A. Lucock[15], A. Lyssoivan[17], J. Maagdenberg[6], A. Maas[2], J. MacGregor[15], P. Macheta[15], G. Maddaluno[5, b], G.P. Maddison[15], P. Maget[2], R. Magne[2], A. Mahdavi[24], J. Mailloux[15], D. Maisonnier[16], J. Manickam[30], G. Mank[7], M.E. Manso[9], P. Mantica[5, d], M. Mantsinen[13], M. Maraschek[8], D. Marcuzzi[5,b], M. Marinucci[5, b], Ph. Marmillod[12], D. Martin[15], M. Martin[15], Y. Martin[12], K.F. Mast[8], M. Mattei[5, c], G.F. Matthews[15], M. Mayer[8], ML. Mayoral[15], D. Mazon[2], G. Mazzone[5, b], E. Mazzucato[30], E. McCarron[15], K. McClements[15], K. McCormick[8], P.A. McCullen[15], D. McCune[30], D. McDonald[15], M. Mead[15], F. Medina[3], A. Meigs[15], W. Melissen[6], L. Meneses[9], F. Meo[8], Ph. Mertens[7], V. Mertens[8], A. Messiaen[17], F. Milani[15], A. Miller[15], S. Mills[15], J. Milnes[15], J. Mlynar[12], I. Monakhov[15], P. Monier-Garbet[2], R. Monk[8], R. Mooney[15], D. Moreau[2], Ph. Moreau[2], P.D. Morgan[15], A.W. Morris[15], J. Morris[15], J.L. Mort[15], D. Mossessian[28], A. M¸ck[8], G. Mueller[14], M. Murakami[29], A. Murari[5, a], D. Murdock[16], Y-S. Na[8], F. Nabais[9], M.F.F. Nave[9], R. Nazikian[30], C. Negus[15], G.F. Neil[15], J.D. Neilson[15], B. Nelson[30], R. Neu[8], W. Nevins[26], G.J. Newbert[15], F. Nguyen[2], K. Nichols[15], A. Nicolai[7], L. Nicolas[2], P. Nielsen[5, a], M. Nightingale[15], H. Nordman[10], J-M. Noterdaeme[8], S. Nowak[5, d], M. O'Mullane[15], J. Ongena[17], T. Onjun[27], J. Orchard[15], F. Orsitto[1, 5], T. Osborne[24], J. Palmer[16], J. Pamela[1, 2], L. Panaccione[5, b], V. Parail[15], A. Parkin[15], B. Parsons[15], R. Pascualotto[1,5], B. Patel[15], I. Pavlenko[17], A.T. Peacock[16], R. Pearce[15], AL. Pecquet[2], A. PedrosaLuna[3], A. Peeters[8], R.D. Penzhorn[14], M. Peres Alonso[9], G. Pereverzev[8], A. Perevezentsev[15], C. Perez von Thun[7], V. Pericoli[5, b], S. Peruzzo[5, a], G. Petravich[19], V. Petrizilka[18], Y. Petrov[32], C. Petty[24], V. Phillips[7], F. Piccolo[15], M. Pick[16], S.D. Pinches[8], T. Pinna[5, b], B. Piosczyk[14], CS. Pitcher[28], R. Pitts[12], V. Plysnin[9], A. Pochelon[12], S. Podda[5, b], P. Polinari[5, b], N. Pomaro[5, a], S. Popovichev[15], C. Portafaix[2], G. Porter[26], A. Pospieszczyk[7], G. Preece[15], R. Prentice[15], R. Prins[6], M. Proschek[11], R. Pugno[8], ME. Puiatti[5,a], K. Purahoo[15], E. Rachlew[10], M. Rainford[15], D. Raisback[15], J. Rapp[1, 7], D. Rasmussen[29], D. Reiser[7], D. Reiter[7], G. Rewoldt[30], TM. Ribeiro[9], V. Riccardo[15], E. Righi[16], F.G. Rimini[2], M. Riva[5, b], D.S. . Robinson[15], S.A. Robinson[15], D.W. Robson[15], M. Roccella[5, b], L. RodriguezRodrigo[3], G. Rogero[2], A. Rogister[7], T. Roguemore[30], A. Rolfe[15], D. Ronden[6], S. Rosanvallon[2], D. Ross[15], M. Rubel[10], F. Ryter[8], S. Saarelma[13], F. Sabathier[2], R. Sabot[2], G. Saibene[16], J.F. Salavy[2], I. Sall[15], J. Sanchez[3], S. Sanders[15], S.G. Sanders[15], D. Sands[15], Y. Sarazin[2], F. Sartori[15], R. Sartori[16], F. Sattin[5,a], O. Sauter[12], C. Sborchia[16], F. Scaffidi-Argentina[1, 14], A. Scarabosio[12], G. Schilling[30], D. Schissel[24], J. Schlosser[2], G. Schmidt[30], W. Schmidt[5, a], C. Sch¸ller[6], B. Schweer[7], J. Schweinzer[8], J.L. Segui[2], L. Semeraro[5, b], G. Sergienko[7], F. Serra[9], S.E. Sharapov[15], S.R. Shaw[15], M. Siegrist[1,12], CA. Silva[9], D. Simpson[15], S. Sipila[13], A.C.C. Sips[8], H. Sjostrand[10], C. Skinner[30], P.G. Smith[15], J. Snipes[28], E.R. Solano[1,3], P. Sonato[5, a], J. Sousa[9], C. Sozzi[5, d], J. Spence[15], E. Speth[8], A. Staebler[8], R. StaffordAllen[15], R. Stagg[15], J. Stakenborg[6], M.F. Stamp[15], P. Stangeby[35], D. Starkey[15], S.A. Stauton-Lambert[15], A. Stephen[15], A. Sterk[6], A.B. Sterk[6], A. Stevens[15], J. Stillerman[24], J. Stober[8], R. Stokes[15], D. Stork[15], J. Strachan[30], B. Stratton[30], K. Stratton[30], P. Stubberfield[15], H.P. Summers[15], E. Surrey[15], D. Sutton[15], W. Suttrop[8], J. Svenson[8], I. Symonds[15], F. Tabares[3], J. Tait[15], T. Tala[13], C. Talarico[5, b], A.R. Talbot[15], C. Taliercio[5, a], U. Tam[14],

C. Tame[15], G. Tardini[8], M. Tardocchi[10], N. Tartoni[5, b], J. Tavernier[2], G. Telesca[17], A.O. Terrington[15], D. Testa[12], P. Testoni[5, e], J.M. Theis[2], J. Thomas[15], P. Thomas[2], H. Thomsen[8], K. Thomsen[16], M. Thumm[14], C. Thyagaraja[15], J. Tichler[6], P. Tigwell[15], T. Tiscornia[15], J.M. Todd[15], M.Z. Tokar[7], Q.M. Tran[12], J.M. Travere[2], G. Tresset[2], V. Tribaldos[3], E. Tsitrone[2], A.A. Tuccillo[5, b], O. Tudisco[5, b], E. Turker[15], M. Turner[4], V. Udintsev[6], B. Unterberg[7], M.P. Valetta[2], M. Valisa[5, a], M. Valovic[15], F. Van Amerongen[6], M. Van de Poll[6], T. Van der Grift[6], D. Van Eester[17], J. Van Gorkorm[6], P. Varela[9], D. Vender[4], G. Veres[19], A. Verhoeven[6], L. Villard[12], E. Villedieu[15], F. Villone[5, a], J.E. Vince[15], M. VonHellermann[6], K. Vulliez[2], M. Wade[24], D. Wagner[8], A. Walden[15], M. Walker[15], B. Walton[15], M.L. Watkins[1, 15], M.J. Watson[15], J. Weiland[10], H. Weisen[12], A. Werner[8], F. Wesner[8], P. West[24], E. Westerhof[6], B. Weyssow[17], M.R. Wheatley[15], A. Whitehead[15], A. Whitehurst[15], D. Whyte[33], S.J. Wicks[15], L. Widdershoven[6], P. Wienhold[7], A. Wilson[15], C. Wilson[15], D. Wilson[15], D.J. Wilson[15], D.W. Wilson[15], R. Wilson[30], M. Wischmeier[12], R. Wolf[7], P. Wouters[17], J.S. Yorkshades[15], C. Young[15], D. Young[15], I.D. Young[15], K. Young[30], L. Zabeo[2], F. Zacek[18], L. Zakharov[30], P. Zanca[5, a], K.D. Zastrow[15], W. Zeidner[8], M. Zerbini[5, b], H. Zohm[8], S. Zoletnik[19], F. Zonca[5, b], W. Zwingman[2].

[1] EFDA Close Support Unit, Culham, *UK*.

[2] Association Euratom-CEA, Cadarache, *France*.

[3] Asociación EURATOM-CIEMAT para Fusión, Madrid, *Spain*.

[4] Dublin City University (DCU), *Ireland*.

[5] Associazione Euratom ENEA sulla Fusione, *Italy* [a] Consorzio RFX Padova, [b] CR Frascati, Roma, [c] CREATE, [d] IFP, Milano, [e] Univ. Cagliari, [f] Univ. Brasimone, [g] Univ. Bologna.

[6] FOM-Rijnhuizen, Association Euratom-FOM, TEC, Nieuwegein, *The Netherlands*.

[7] Institut fur Plasmaphysik, Forschungszentrum Julich, Trilateral Euregio Cluster, D-52425 Julich, *Germany*.

[8] Max-Planck-Institut für Plasmaphysik, EURATOM-Assoziation, D-85748 Garching, *Germany*.

[9] Associão EURATOM/IST, Centro de Fusão Nuclear, 1049-001 Lisbon, *Portugal*.

[10] EURATOM-VR Association, Swedish Research Council, Stockholm, *Sweden*.

[11] Österreichische Akademie der Wissenschaften (ÖAW), *Austria*.

[12] Centre de Recherches en Physique des Plasmas, Association EURATOM-Confédération Suisse, EPFL, 1015 Lausanne, *Switzerland.*

[13] Helsinki U. of Technology, Tekes-Euratom Assoc., PO Box 2200, FIN-02015 HUT, *Finland.*

[14] Forschungszentrum Karlsruhe (FZK), *Germany*.

[15] Euratom/UKAEA Fusion Association, Culham, Abingdon, *UK*.

[16] EFDA Close Support Unit, Garching, *Germany*.

[17] Association Euratom-Belgian State, LPP-ERM/KMS, *Belgium*.

[18] Institute of Plasma Physics (IPP), Academy of Sciences, *Czech Republic.*

[19] Hungarian Academy of Sciences (HAS), *Hungary*.

[20] Ministry of Education and Research (MEC), *Romania*.
[21] Université de Nice-Sophia-Antipolis, Nice, *France*.
[22] Imperial College, London, *UK*
[23] Colorado School of Mines (CSM), Colorado, *USA*.
[24] General Atomics, San-Diego, California, *USA*.
[25] Institue for Fusion Studies, University of Texas, Austin, *USA*.
[26] Lawrence Livermore National Laboratory, California, *USA*.
[27] Le High University, *USA*.
[28] Massachusetts Institute of Technology, Cambridge, Massachusetts, *USA*.
[29] Oak Ridge National Laboratory, Tennessee, *USA*.
[30] Princeton Plasma Physics Laboratory, New-Jersey, *USA*.
[31] Sandia National Laboratory, *USA*.
[32] Texas A&M University, College Station, *USA*.
[33] University of California, San Diego, *USA*.
[34] University of Maryland, *USA*.
[35] University of Toronto, *Canada*.
[36] University of Wisconsin, Madison, *USA*.

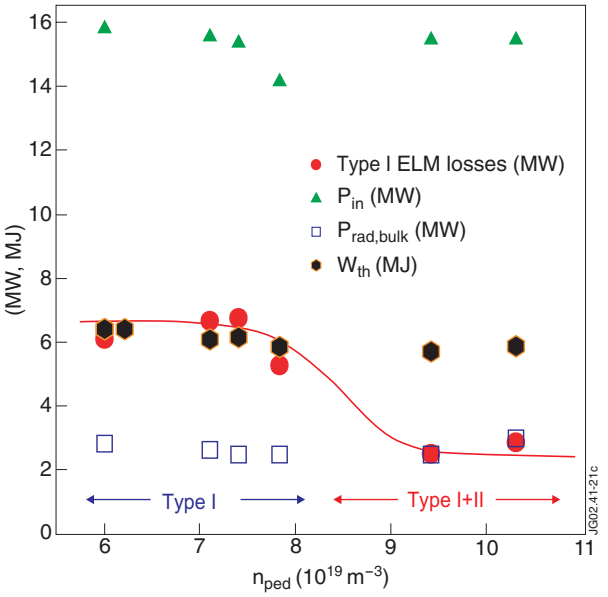

Figure 1: Loss power balance of a gas scan. At highest pedestal density, average ELM losses are reduced, indicating an additional loss mechanism in between ELMs. Also, see Section 2.3.1

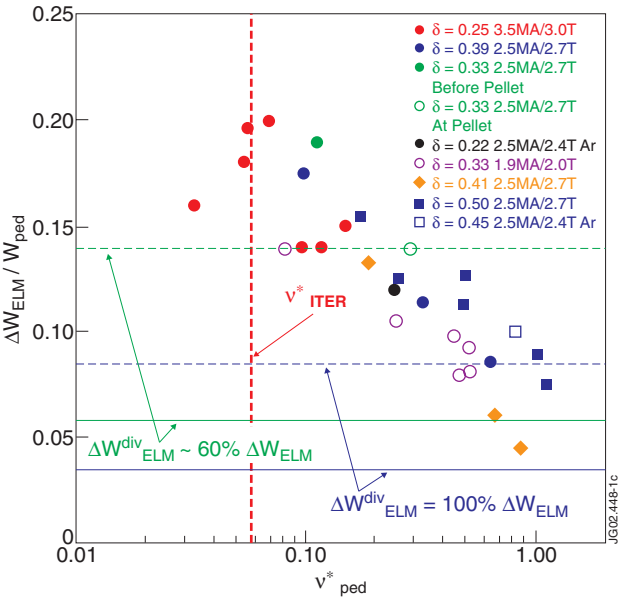

Figure 2: Scaling of Type I ELM size with pedestal collisionality

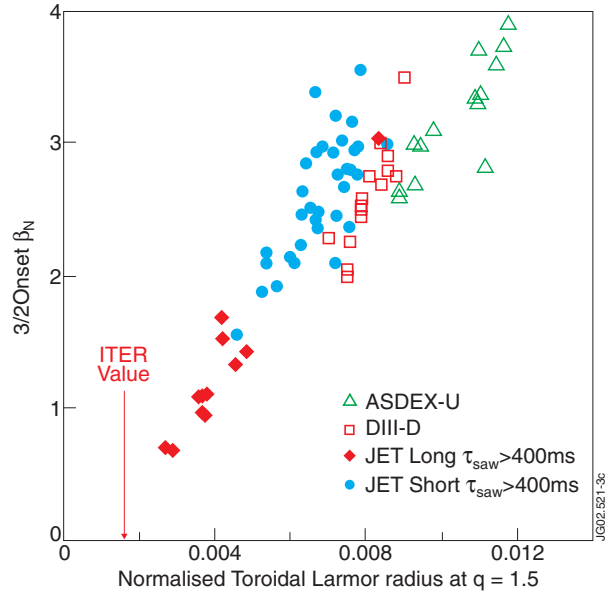

Figure 3: Onset β_N for 3/2 NTM, as a function of ρ^*_i (toroidal Larmor radius at q=3/2 divided by minor radius). The DIII-D and ASDEX-U data are corrected for collisionality dependence (see Figure 6 of Ref. [34]), whereas the JET data shows no significant collisionality dependence

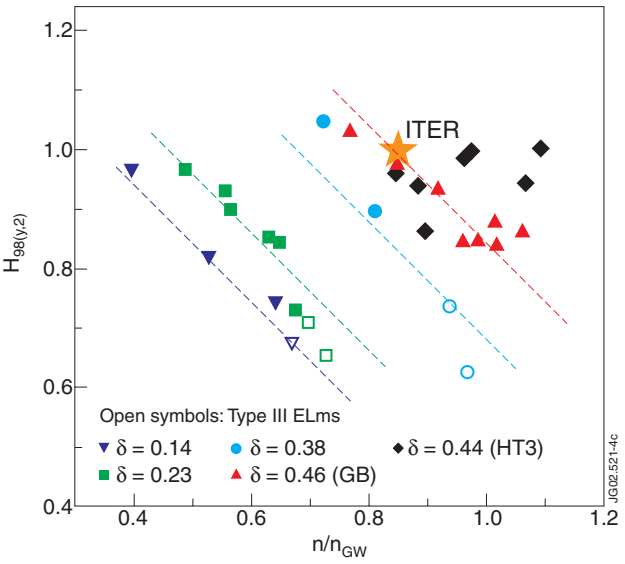

Figure 4: H factor vs. Greenwald factor, as a function of triangularity, δ

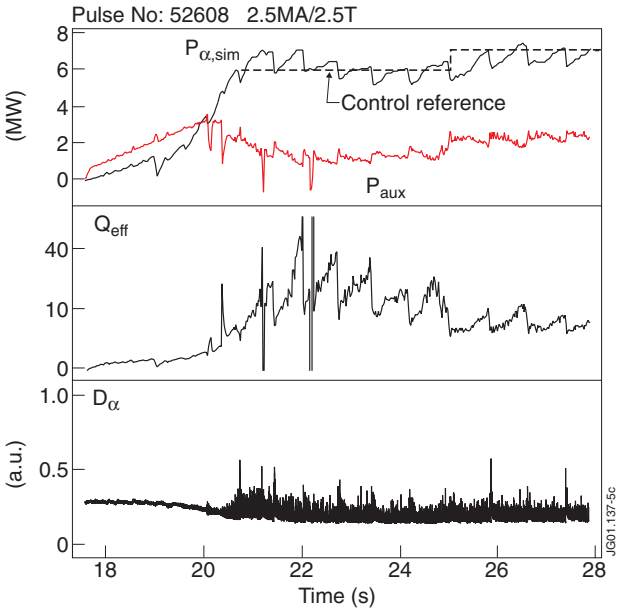

Figure 5: Controlled step-up of $P_{\alpha,\,sim}$, achieved via feedback control of P_{aux}

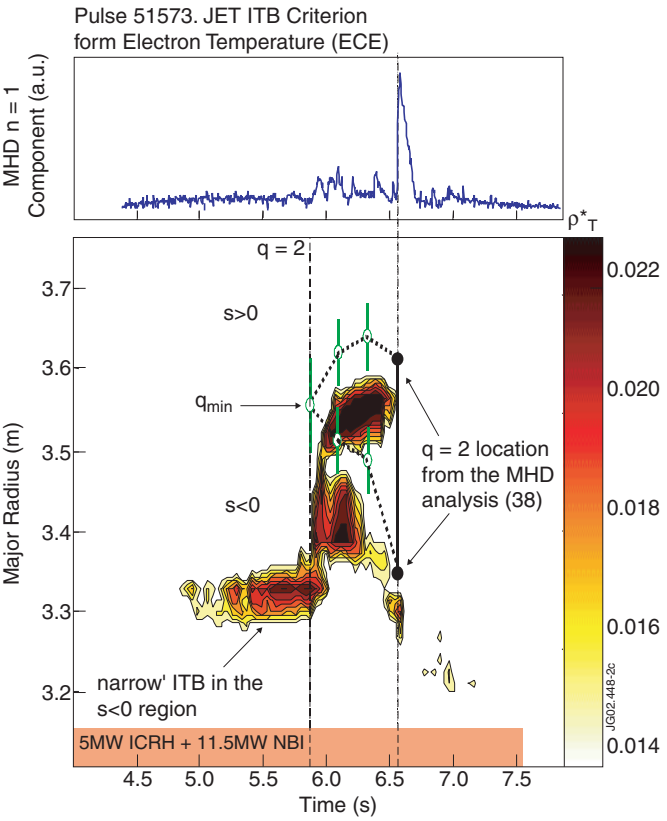

Figure 6: Plot of ITB criterion versus time and plasma radius. When q_{min} crosses 2 the barrier is broadened (radius increased by ~30 cm) and two barriers follow the evolution of the q = 2 surfaces. The time when q_{min} crosses two is confirmed from the excitation of Alfvén cascades

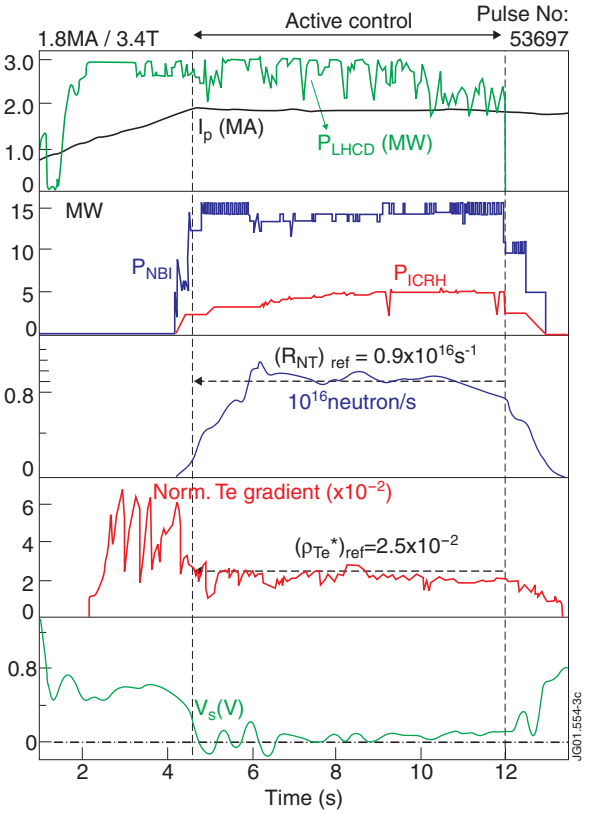

Figure 7: Time evolution of the main parameters of a discharge with combined ρ^*_{Te} and R_{NT} feedback control using ICRH and NBI powers (#53697, B_t=3.4 T, I_p=1.8 MA)